

Article

Microbial Mineralization-Based Rapid and High-Strength Simultaneous Repair of Surrounding Rock Fracture Zones and Lining Cracks

Rongzheng Zhang¹, Shixia Zhang¹, Zhichao Song¹, Danyi Shen¹ and Chuangzhou Wu^{1,2,*}

¹ Institute of Port, Coastal and Offshore Engineering, Ocean College, Zhejiang University, Zhoushan 316021, China; rz_zhang@zju.edu.cn (R.Z.); zhichao_song@zju.edu.cn (Z.S.); shendanyi@zju.edu.cn (D.S.)

² Key Laboratory of Western China's Mineral Resources and Geological Engineering, Ministry of Education, Chang'an University, Xi'an 710054, China

* Correspondence: ark_wu@zju.edu.cn

Abstract: Grouting technology based on microbial mineralization represents a novel approach to enhancing the properties of rock and soil. Widely studied for its combination of high efficiency and environmental friendliness, this method improves the strength and permeability of rock and soil. In this study, a novel approach involving bioslurry + filling particles was proposed to reinforce sand columns. It was observed that the addition of filling particles provided new nucleation sites for crystallization, significantly enhancing the cementation effect of sand particles. After 3 days of grouting treatment, sand columns containing 10% filling particles exhibited an order of magnitude reduction in permeability with the unconfined compressive strength (UCS) reaching 2.5 MPa, more than twice that of sand columns reinforced with bioslurry alone. Additionally, this study presented a method for the simultaneous repair of sand particles and concrete cracks. Results indicated that after 3 days of the grouting treatment, the interfacial shear strength between sand columns and concrete reached 100 kPa. Moreover, for concrete with crack apertures less than 1 mm, the permeability coefficient was reduced by over 80%, while the recovery ratio of the splitting tensile strength reached 64.2%. These findings highlight the potential of microbial mineralized grouting technology in addressing practical challenges, providing a foundation for the rapid and high-strength simultaneous repair of tunnel-surrounding rock fracture zones and lining cracks.

Keywords: microbial mineralization; surrounding rock fracture; lining cracks; simultaneous repair; rapid and high strength



Citation: Zhang, R.; Zhang, S.; Song, Z.; Shen, D.; Wu, C. Microbial Mineralization-Based Rapid and High-Strength Simultaneous Repair of Surrounding Rock Fracture Zones and Lining Cracks. *Sustainability* **2024**, *16*, 3751. <https://doi.org/10.3390/su16093751>

Academic Editor: Alireza Ahangar-Asr

Received: 28 January 2024

Revised: 18 March 2024

Accepted: 22 March 2024

Published: 30 April 2024



Copyright: © 2024 by the authors. Licensee MDPI, Basel, Switzerland. This article is an open access article distributed under the terms and conditions of the Creative Commons Attribution (CC BY) license (<https://creativecommons.org/licenses/by/4.0/>).

1. Introduction

With the extensive development of tunneling projects, tunnels frequently encounter fracture zones during construction, where the low rock strength and high surrounding rock pressure compromise structural stability. Over time, these conditions lead to various issues in tunnel linings, with cracking being the most severe. Cracks in the tunnel lining not only destabilize structures but also facilitate groundwater leakage, causing reinforced concrete corrosion and jeopardizing the tunnel's stability [1–3]. Grouting is a common civil engineering technique used to reinforce fractured rock and cracks in seal lining, typically using cement or chemical slurries. However, the poor flowability of cement slurry and its dependence on mechanical equipment, together with the toxicity and environmental impact of most chemical slurries, highlight the need for a green, fast, and efficient alternative.

In recent years, microbial mineralization-based grouting technology has emerged as a promising solution, leveraging microbially induced calcium carbonate precipitation (MICP) to consolidate and strengthen rock and soil [4–6]. This technique addresses pores or

cracks in rock and soil, offering compatibility with concrete, excellent flowability, reduced mechanical dependence, and environmental friendliness.

Several studies have explored MICP reinforcement in sandy foundations. Whiffin [7] pioneered microorganism-based soil cementation, while subsequent research by DeJong et al. [8] demonstrated increased shear capacity in MICP-treated sand. However, challenges such as non-uniform calcium carbonate distribution prompted the development of the two-phase injection method by Whiffin and Van Paassen [9], subsequently refined by others [10–14]. Bioslurry, incorporating pre-formed calcium carbonate crystals with embedded urease bacteria, has emerged as a viable alternative, particularly effective in porous sands [15–17].

MICP repair of concrete cracks has also been investigated. Two primary repair methods were employed: (1) the self-repair method involves incorporating repair materials into the concrete prior to crack formation. Once a crack appears, a self-repair reaction is initiated to seal it [18]. (2) In the passive repair method, cracks are filled with calcium carbonate crystals generated by MICP subsequent to crack formation [19]. Numerous studies demonstrate that these MICP-induced calcium carbonate crystals effectively fill concrete cracks, reducing permeability and enhancing concrete strength and durability [20–22]. However, the simultaneous repair of tunnel rock and lining cracks remains unexplored.

This study conducts microbial grouting repair experiments on sand particles and concrete cracks using bioslurry and calcium sand-filling particles. It explores the cementing effect on sand particles and the simultaneous repair effect of sand particles and concrete cracks, with the aim of providing a basis for the application of microbial-mineralization grouting technology in the rapid and high-strength simultaneous repair of tunnel rock fracture zones and lining cracks.

2. Materials and Methods

2.1. Preparation of Bacterial Solution and Cementation Solution

The urease-producing bacterial (UPB) strain utilized in this study was *Bacillus pasteurii* (DSM 33). The bacterial culture medium was formulated with 20 g/L yeast extract, 10 g/L $(\text{NH}_4)_2\text{SO}_4$, and 15.75 g/L Tris Buffer at pH 9.0. The optical density (OD600) of the bacterial solution ranged from 1.4 to 1.6, with urease activity measuring between 10 and 12 U/mL. The cementing solution comprised 1 mol/L CaCl_2 and 1 mol/L urea.

2.2. Preparation of Bioslurry

The cement solution was mixed with the bacterial solution in a ratio of 1:4 and stirred at 400 rpm for approximately 12 h. The reaction was sufficiently complete to produce a suspension containing calcium carbonate crystals, as shown in Figure 1a. The suspension was placed in a refrigerator at 4 °C for about 8 h to precipitate and obtain sedimented crystals, i.e., bioslurry, as shown in Figure 1b.

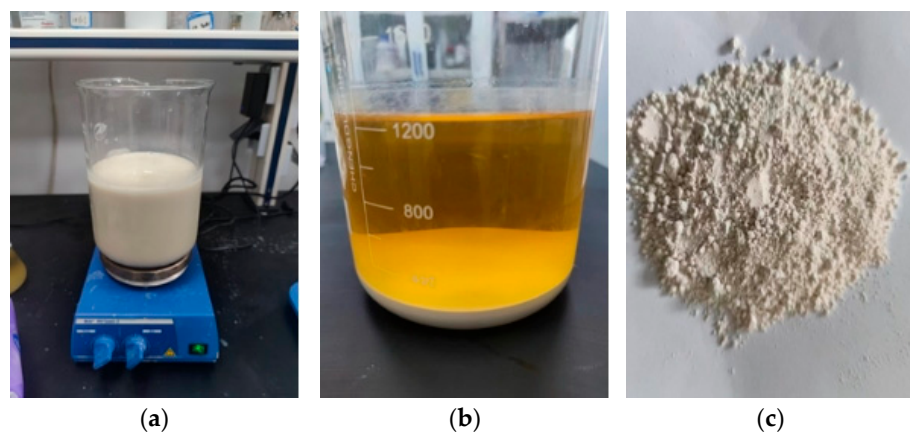


Figure 1. Test materials. (a) Suspension with calcium carbonate crystals. (b) Sedimented crystals, i.e., bioslurry. (c) Calcareous sand filling particles.

The main component of calcareous sand is calcium carbonate. Therefore, in this study, calcareous sand was ground into fine particles and added to the bioslurry to examine the impact of filling particles on microbial-mineralization grouting. The calcareous sand used in this study was sourced from oceanic islands, with the particle size of the ground-filling particles measuring less than 0.1 mm, as depicted in Figure 1c.

2.3. Methods of Preparing Sand and Concrete Samples

This study comprises two groups of tests: sand particle cementation tests and simultaneous reinforcement tests of sand particles and concrete cracks.

For the sand particle cementation test, quartz sand with a density of 1.70 g/cm³ and particle size ranging from 2 to 4 mm were utilized. Prior to grouting, 300 g of sand, along with a specific quantity of the bioslurry and filling particles, were mixed and added to the mold in batches. The mixture was vibrated to form a sand column measuring 50 mm in diameter and 100 mm in height.

In the simultaneous sand particle and concrete crack reinforcement tests, concrete samples were prepared using normal silicate cement, ISO standard sand, and distilled water, with the water-cement ratio controlled at 0.4 and the sand-cement ratio at 2.5. The samples were mixed and poured into PVC molds measuring 50 mm in diameter and 30 mm in height. After curing for 28 days in a laboratory environment (24 °C), the specimens were split using a universal testing machine, and the original split tensile strength (T_0) was recorded. Penetrating cracks were induced, and crack width was measured using a crack viewer. Ten points were uniformly measured along the fracture direction, with the average value taken as the sample's crack width. Two types of cracks were produced: narrow cracks (0.1 mm to 0.5 mm) and wide cracks (0.5 mm to 1 mm). The cracked concrete specimens were then bonded to the PVC molds of the sand columns to obtain complete reinforced specimens. In this series of tests, two methods were employed to prepare the sand columns: the mixing method (mix) mentioned in the sand particle cementation test, and a direct injection method (inject). In the inject method, the bioslurry was injected from the top of the molds, flowed through the sand particles and concrete cracks, and was finally discharged from the bottom. This process was repeated 5–8 times to ensure most of the calcium carbonate crystals in the bioslurry remained in the sand particles and concrete cracks.

2.4. Unsaturated Grouting Program and Device

In the unsaturated state, the capillary effect facilitates increased precipitation of calcium carbonate crystals at the contact points between sand particles. Thus, this study employs the unsaturated grouting method.

The test program for sand particle cementation, detailed in Table 1, aims to investigate the impact of bioslurry quantity, filling particles, and grouting time on cementation effectiveness. To enhance the credibility of the test, three specimens were prepared for each group, and the test data were averaged across the trio, giving a total of 27 samples. The schematic diagram of the injection device is provided in Figure 2a. A layer of cotton cloth was placed at the top of the sand column, through which CS was injected from the top of the sand sample. It traversed the sand particles, exiting through a small hole at the bottom, and was pumped back to the top by a peristaltic pump to achieve cyclic grouting. The grout flow rate was maintained at 10 mL/min, and the CS was changed every 24 h.

Table 1. The test program for sand particle cementation.

Sample NO.	Content of Bioslurry (%)	Content of Filling Particles (%)	Grouting Duration (Day)
A-1			1
A-2	5	0	2
A-3			3

Table 1. Cont.

Sample NO.	Content of Bioslurry (%)	Content of Filling Particles (%)	Grouting Duration (Day)
B-1	5	5	1
B-2			2
B-3			3
C-1	5	10	1
C-2			2
C-3			3

The test program for the simultaneous repair of sand particles and concrete cracks aims to investigate the impact of the crack opening and bioslurry addition method on the strengthening effect of the specimens (Table 2). Two specimens were prepared for each group, resulting in a total of 8 specimens. The schematic diagram of the grouting apparatus is presented in Figure 2b. CS was injected from the top of the sand specimen, passing through the sand column and concrete, before exiting from the bottom and being pumped back to the top of the sand column to achieve cyclic grouting. The grout flow rate was maintained at 10 mL/min and the solution was changed every 24 h.

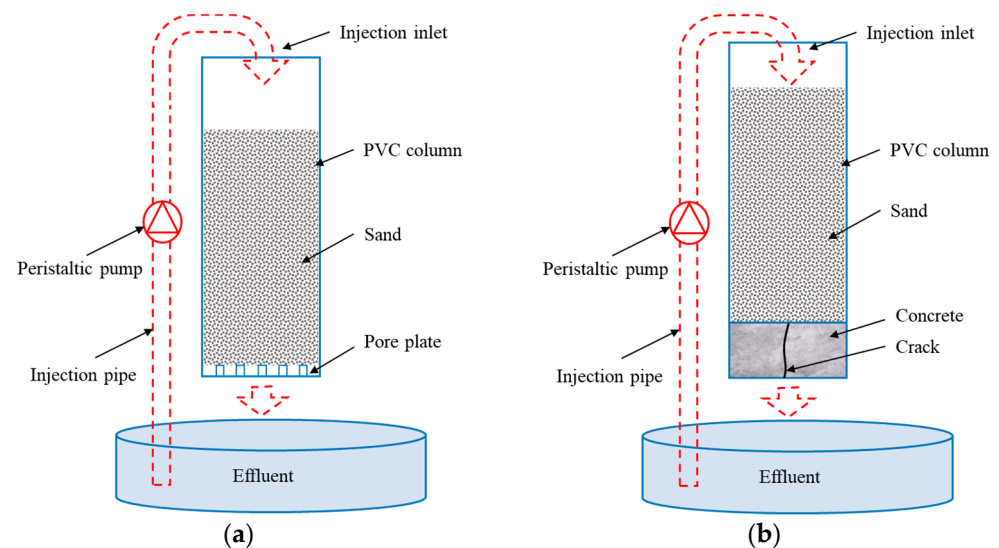


Figure 2. Schematic diagram of the grouting device. (a) Sand particle cementation test. (b) Simultaneous repair test of sand particles and concrete cracks.

Table 2. The test program for simultaneous repair of sand particles and concrete cracks.

Sample NO.	Content of Bioslurry (%)	Crack Aperture (mm)	Method	Grouting Duration (Day)
NI	5	0.1–0.5	Inject	3
NM			Mix	
WI		0.5–1.0	Inject	
WM			Mix	

Note: N: Narrow aperture; W: Wide aperture; I: Inject bioslurry directly; M: Mix bioslurry with sand.

2.5. Testing for Permeability

After the completion of the grouting process, the sand column was carefully removed from the PVC mold and gently rinsed with more than five times the volume of deionized water to eliminate residual soluble salts from the surface. Subsequently, the specimens were placed in an oven and dried at 60 °C for 24 h. The permeability coefficient of the

sand column before grouting (k_0) and the permeability coefficient after grouting (k_a) were determined using the constant head method. The diagram of the permeability test device is illustrated in Figure 3. In this setup, the sample is positioned within the test device with its bottom immersed in a tank filled with water. The tank features a hole to facilitate water outflow, thereby maintaining a constant water head on the sample. Parameters such as L (sample height), A (cross-sectional area of the sample), and h (constant water head) were directly measured before the test. Throughout the permeability test, water was continuously supplied from the top of the PVC pipe, while the time (t) and water quantity (Q) in the water tank were recorded. According to Darcy's law, the permeability coefficient k of the specimen can be obtained as follows:

$$k = \frac{QL}{Aht}$$

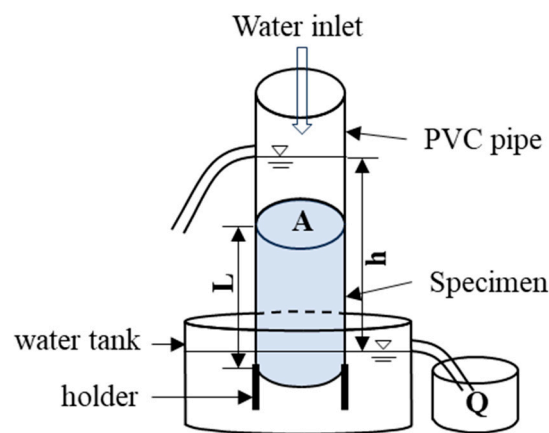


Figure 3. Schematic diagram of the permeability test setup.

Subsequently, the difference in the permeability coefficient (Δk) before and after grouting is calculated ($\Delta k = k_0 - k_a$), and the ratio of this difference to the permeability coefficient before grouting yields the permeability reduction ratio (R), i.e., $R = \Delta k/k_0$. Permeability testing of the concrete specimens follows a similar procedure to that of the sand columns.

2.6. Testing for Unconfined Compressive Strength (UCS) and Calcium Carbonate Content (CCC)

Following the drying of the sand columns, axial loading was exerted on them using a universal testing machine at a loading rate of 1.0 mm/min, adhering to the protocol outlined in the ASTM D2166 [23] report. The unconfined compressive strength (UCS) of the sand columns was then recorded upon completion of the loading process.

Sand particles were sampled from the top, middle, and bottom positions of the sand column, and the calcium carbonate content (CCC) was assessed using the acid washing method. The average value of the CCC obtained from these three positions was considered representative of the sand column's CCC.

2.7. Testing for Interfacial Shear Strength and Split Tensile Strength (STS)

In the simultaneous repair test of sand particles and concrete, the adhesive properties of the interface between the repaired sand particles and concrete were investigated through interface shear strength testing. As illustrated in Figure 4a, the specimens were affixed to a custom fixture and subjected to loading using a universal testing machine at a rate of 1.0 mm/min.

Additionally, the repaired concrete underwent a splitting tensile strength test, following the procedure outlined in ASTM C496 [24]. As depicted in Figure 4b, the concrete specimens were positioned on the loading table of the universal testing machine, also at a loading rate of 1.0 mm/min. The ratio of the post-repaired splitting tensile strength to

the initial splitting tensile strength was defined as the splitting tensile strength recovery rate. Furthermore, the ratio of the split tensile strength of the repaired concrete (T_a) to the original split tensile strength (T_0) was determined as the split tensile strength recovery rate (H), calculated as $H = T_a/T_0$.

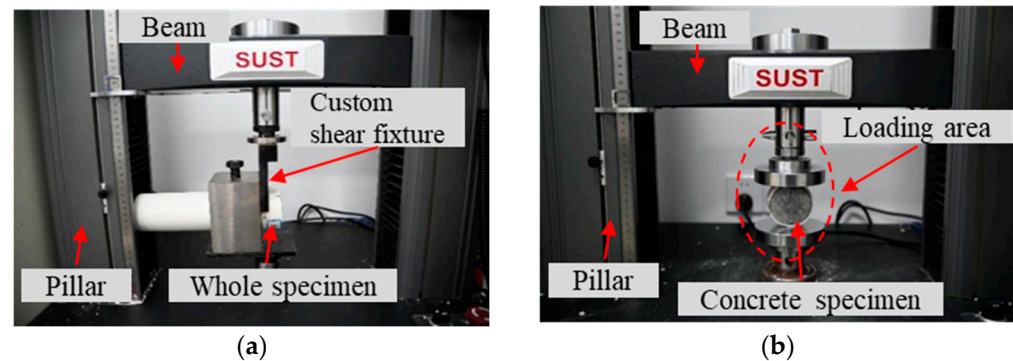


Figure 4. Strength tests of specimens. (a) Shear strength at the interface of sand column and concrete. (b) Split tensile strength of concrete.

2.8. Analysis of Microstructure

Sigma 500 scanning electron microscopes (manufactured by Carl Zeiss in Oberkochen, Germany) were utilized at various magnifications ($500\times$, $1.00K\times$, $5.00K\times$) to observe the morphology of CaCO_3 between cemented sand particles and CaCO_3 on the inner walls of concrete cracks.

3. Results and Discussion

3.1. Sand Particle Cementation Test

3.1.1. CCC and UCS

The UCS and CCC of the reinforced sand columns with different filling contents are illustrated in Figure 5. It is evident that both the CCC and UCS of the sand columns in groups A, B, and C increased with prolonged grouting time, indicating a positive correlation between UCS and CCC. In the case of Group A sand columns containing only 5% bioslurry, the columns were inadequately shaped for UCS testing after just 1 day of grouting due to the low injection of CS and minimal microbial-mineralization reaction, resulting in limited calcium carbonate precipitation within the sand column. After 2 days of grouting, the sand column achieved formation and a UCS of up to 0.65 MPa, increasing to nearly 1.0 MPa after 3 days of grouting. Figure 6 depicts the UCS of the sand column over the grouting time, demonstrating that higher filler content corresponds to increased calcium carbonate content and UCS for the same grouting duration. Compared to Group A with only 5% bioslurry, the UCS of Group B with 5% filling particles was 1.5 to 2 times higher, while Group C with 10% filling particles exhibited more than a 2-fold increase in UCS compared to Group A. In particular, the UCS of Group C with 10% filling particles reached 1 MPa after only 1 day of grouting and increased to 2.5 MPa after 3 days of grouting.

UCS increased with the increase in CCC, making a significant contribution to strength enhancement, which is consistent with previous studies [25]. However, in this study, the strength contribution stems not only from bioslurry and calcium carbonate post-CS injection but also from the addition of fine particles. As depicted in Figure 6, when the grouting time extended to 3 days, the sample strength with 10% fine particles added exceeded that of the sample with 5% fine particles. This enhancement is attributed to the added fine particles providing more nucleation sites for bacteria, fostering the generation of additional calcium carbonate crystals, and filling the pores between the coarse sand particles. This effect is achieved without the need for multiple treatments, unlike traditional MICP. For instance, Konstantinou et al. [26] conducted 16 cycles of two-phase biogrouting with 1.82 mm coarse sand particles, resulting in a sample strength of 2.0 MPa. Similarly, Cheng et al. [27] utilized

the one-phase biogrouting method, but still required 6 days to achieve a UCS of 2.5 MPa for fine sand samples. In a subsequent study, Pan et al. [16] employed bioslurry for grouting coarse sand particles, resulting in a calcium carbonate content of 30% and a corresponding UCS of 1.8 MPa after 8 days of grouting. In the current study, fine particles were added to further enhance these outcomes, resulting in a calcium carbonate content of 20% and a UCS of 2.5 MPa after 3 days of grouting, thus enabling the rapid and high-strength reinforcement of coarse particles.

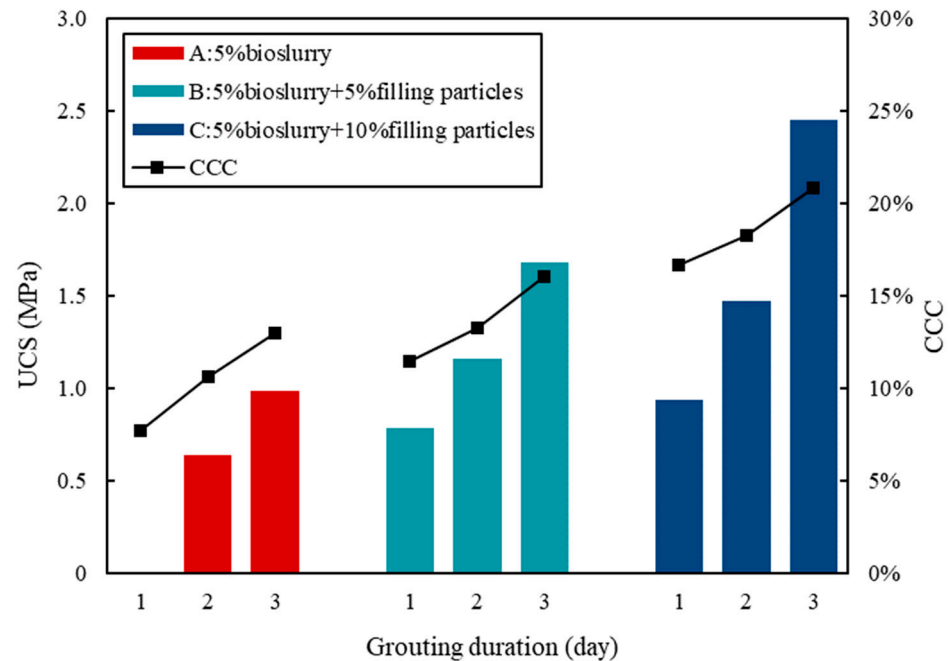


Figure 5. UCS and CCC of sand columns.

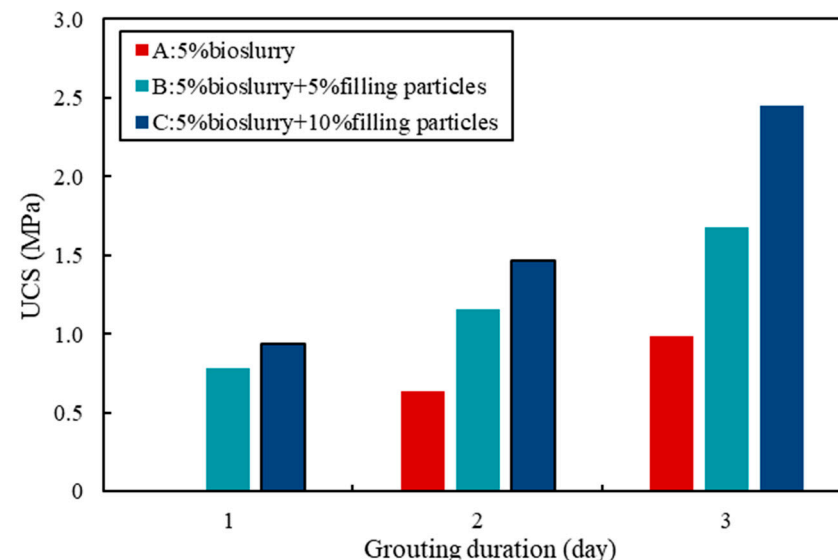


Figure 6. UCS of sand column with grouting duration.

3.1.2. Permeability Reduction Ratio

Figure 7 depicts the variation in the permeability reduction ratios over grouting time for reinforced sand columns with different filler contents. Once again, the permeability data for the Group A specimen was absent due to the specimen's incomplete formation after 1 day of grouting. As observed from Figure 7, the permeability of sand columns

subjected to microbial-mineralization grouting can be reduced by more than 80%. Moreover, as the grouting time extends, the permeability reduction ratio increases, signifying a gradual enhancement in the permeability resistance of the sand columns. Under equivalent grouting durations, the degree of permeability reduction in Group C sand columns was the most pronounced, with the permeability coefficient decreasing by an order of magnitude. In other words, the permeability resistance of Group C sand columns was the greatest, followed by Group B, and the lowest for Group A. This highlights the effectiveness of incorporating filling particles to enhance the microbial grouting treatment effect and increase the permeability resistance of sand columns.

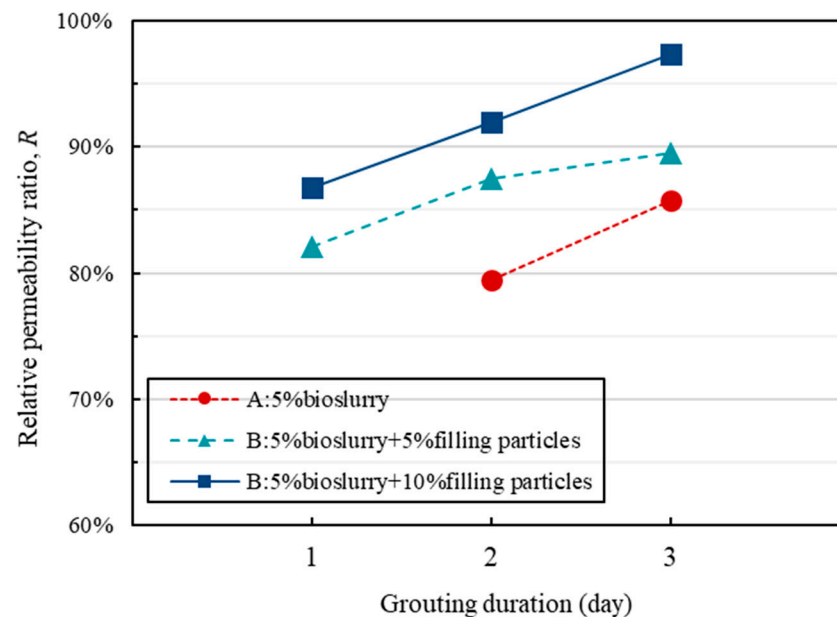


Figure 7. Permeability reduction ratio of sand column over grouting time.

3.1.3. Microstructure

Figure 8 presents SEM images of sand particles treated using two different methods: one with bioslurry alone and the other with bioslurry combined with filling particles. In the left panel of Figure 8a, calcite crystals of various sizes are visible on sand samples treated solely with bioslurry. The smaller crystals originate from the prefabricated bioslurry, while the larger crystals form through the mineralization process induced by the injected CS. These calcium carbonate crystals are densely packed and embedded, as depicted in the locally magnified image on the right side of Figure 8a. Importantly, these crystals exhibit tight bonding to the sand particles, facilitating effective cementation between them. Figure 8 presents SEM images of sand particles treated using two different methods: one with bioslurry alone and the other with bioslurry combined with filling particles. In the left panel of Figure 8a, calcite crystals of various sizes are visible on sand samples treated solely with bioslurry. The smaller crystals originate from the prefabricated bioslurry, while the larger crystals are formed by the mineralization process induced by the injected CS. These calcium carbonate crystals are densely packed and embedded, as depicted in the locally magnified image on the right side of Figure 8a. Importantly, these crystals are tightly bound to the sand particles, facilitating effective cementation between them.

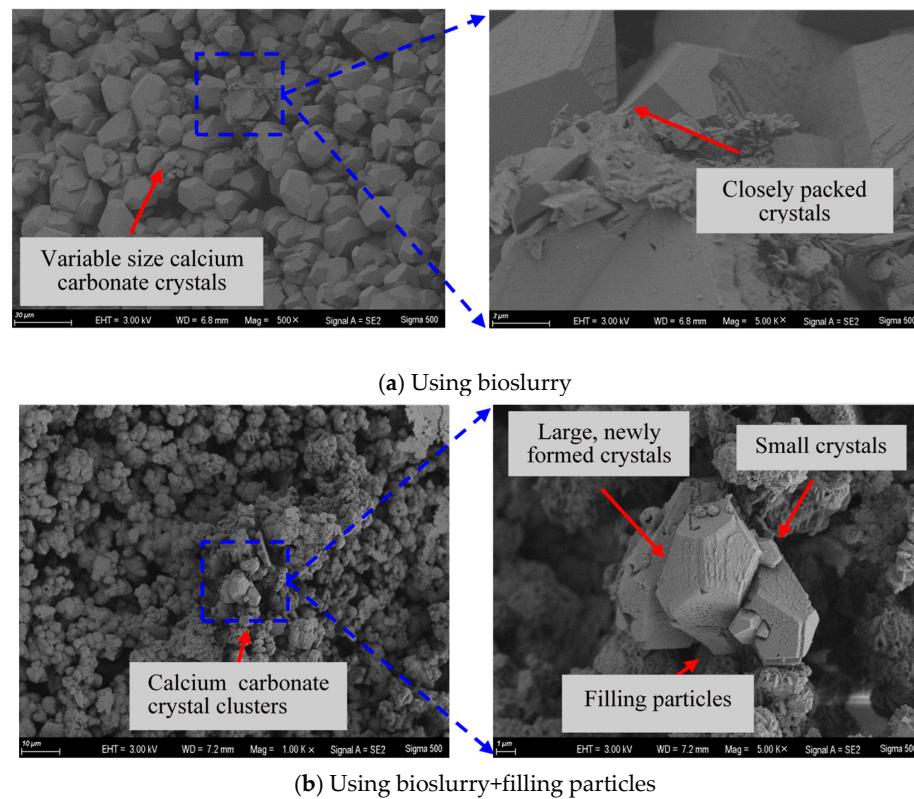


Figure 8. SEM images of sand particles.

3.2. Simultaneous Repair Test of Sand Particles and Concrete Cracks

3.2.1. Apparent Analysis

Figure 9 presents the complete specimen of sand particles and concrete after grouting treatment, clearly indicating the successful cementation of the sand column and concrete. Following shearing, the sand column was separated from the concrete to obtain individual concrete specimens. Figure 10 illustrates the top and bottom surface morphology of the concrete before and after grouting. A notable observation from Figure 10 is the reduction in the crack openings of the untreated concrete specimens after the microbial grouting treatment. Furthermore, when comparing the top and bottom surfaces of the concrete, it becomes apparent that the top surface (i.e., the interface between the concrete and the sand column) is coated with a layer of calcium carbonate precipitate and bonded with a small amount of sand particles. In contrast, the bottom surface is only partially filled with calcium carbonate precipitate. This disparity can be attributed to the grouting process, wherein bioparticles and CS initially flow through the interface before permeating downwards through the interior of the cracks.

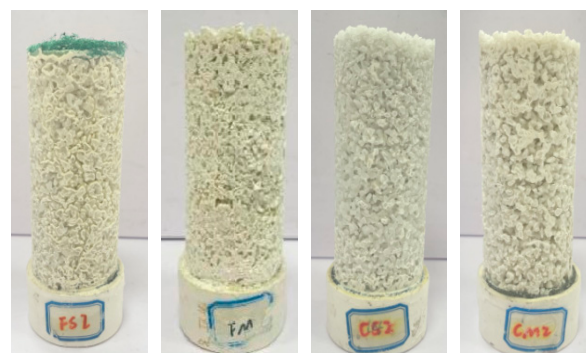


Figure 9. The whole specimen of sand particles and concrete after grouting treatment.

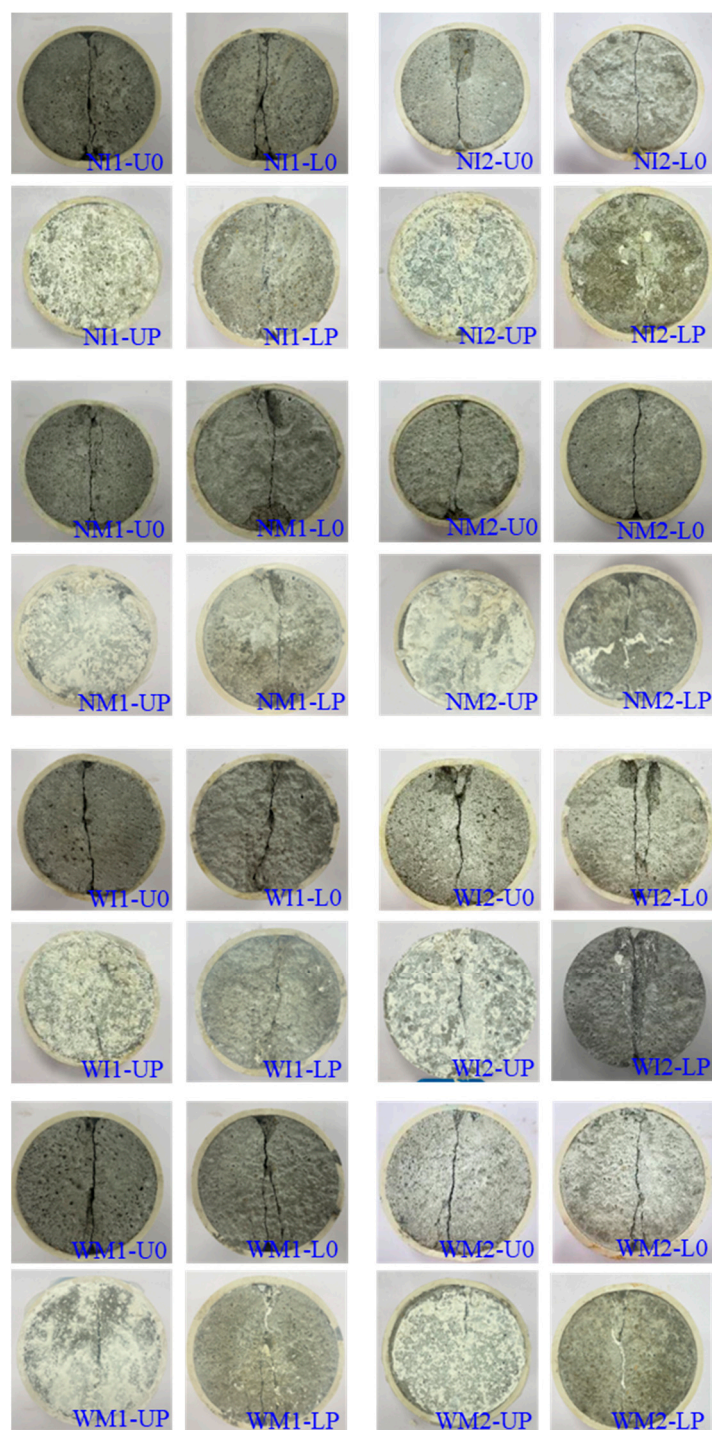


Figure 10. The upper and lower surface morphology of the concrete before and after grouting. Note: U0 and UP denote the upper surface of concrete before and after treatment, respectively; L0 and LP denote the lower surface of concrete before and after treatment, respectively (due to missing records, sample WM2-LP is the lower surface of the concrete form after splitting damage).

The concrete was split again to assess the distribution of calcium carbonate within the concrete cracks. Figure 11 illustrates the internal morphology of the concrete cracks after splitting, revealing that, for most specimens, the calcium carbonate precipitates were predominantly and uniformly distributed on both sides of the cracks. However, a few specimens, such as NM1 and WM2, exhibited an uneven distribution of calcium carbonate.

This irregular distribution could possibly be due to the clogging caused by the small aperture of the cracks in the concrete.

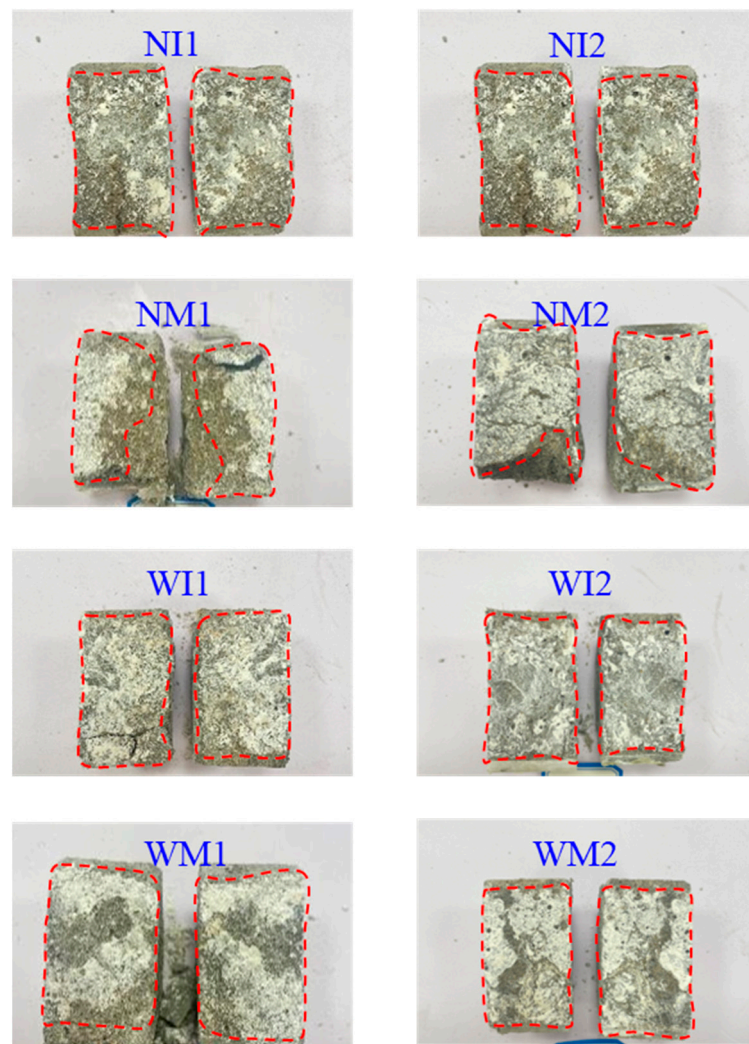


Figure 11. The internal morphology of the concrete cracks after splitting.

3.2.2. Interface Shear Strength

Figure 12 illustrates the interface shear strength of sand columns and concrete, with CCC indicating the calcium carbonate content associated with the sand column in the concrete. While some data were missing due to damage to the sand columns at non-interface points during shear, data were provided for samples derived from concrete with two crack openings using two methods of bioslurry addition. As depicted in Figure 12, a bond strength existed between the sand particles and the microbially grouted concrete, which can be categorized into two scenarios based on the crack opening: for cracks with openings of 0.1–0.5 mm, the interface shear strength reached up to 100 kPa, whereas, for cracks with openings of 0.5–1.0 mm, the interface shear strength was approximately 20 kPa. Remarkably, the method of bioslurry addition does not significantly affect the interfacial shear strength. Furthermore, the interfacial shear strength and calcium carbonate content of samples with crack openings of 0.1–0.5 mm were higher than those of samples with crack openings of 0.5–1 mm. This observation may be attributed to the grouting process, wherein both the bioslurry and CS flow from the upper part of the sand column through the interface into the concrete crack. Compared to samples with larger crack openings, samples with smaller crack openings exhibited lower permeability, resulting in a greater

deposition of the bioslurry at the interface, increased calcium carbonate precipitation, and consequently higher interfacial shear strength.

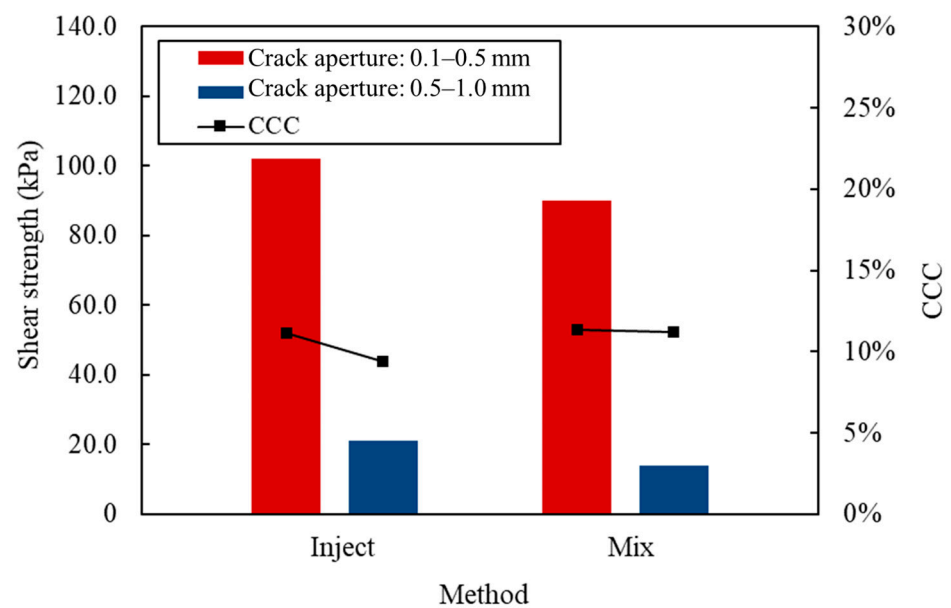


Figure 12. The interface shear strength of sand columns and concrete.

3.2.3. Permeability of Concrete

Figure 13 depicts the relationship between the permeability reduction ratio of concrete and the calcium carbonate content of sand columns. Notably, the method of adding bioslurry was found to have no significant effect on the permeability reduction ratio of concrete during the tests; thus, it will not be further discussed. The data in Figure 13 revealed that when the CCC of the sand column was below 15%, the permeability reduction ratio of concrete remained below 80%. Conversely, when the CCC exceeded 15%, the permeability reduction ratio of concrete surpassed 80%. Both wide-cracked and narrow-cracked concrete exhibited increased permeability reduction ratios with higher calcium carbonate content in the sand column, demonstrating a similar trend between the two types of concrete.

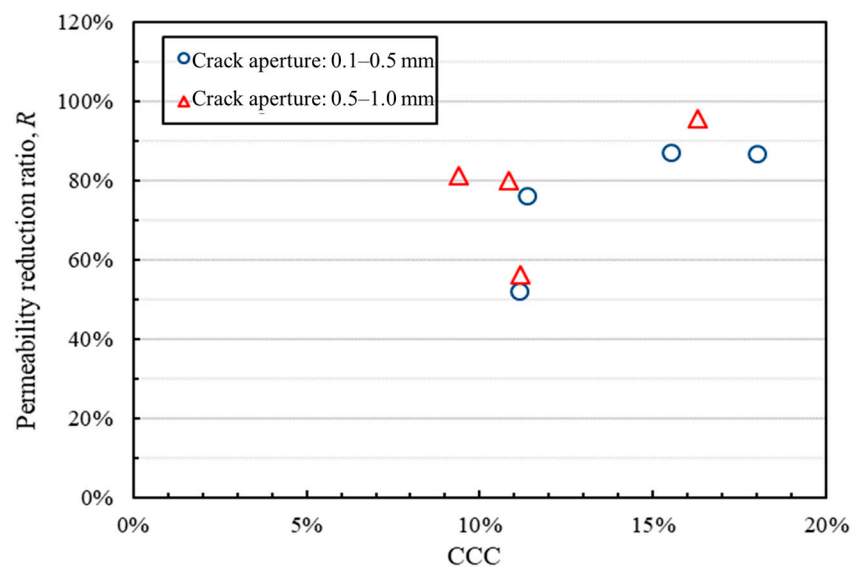


Figure 13. Relationship between permeability reduction ratio of concrete and calcium carbonate content in sand columns.

3.2.4. Splitting Tensile Strength

Figure 14 illustrates the relationship between the splitting tensile strength recovery ratio of concrete and the calcium carbonate content in sand columns. Generally, a higher CCC in the sand column corresponded to a higher recovery ratio of the concrete. For narrow-cracked concrete specimens, the initial splitting tensile strength ranged from 3 to 6 MPa, with repaired splitting tensile strength ranging from 2 to 3 MPa. The tensile strength recovery ratio varied from 50% to 70% with a peak of 64.2%. Wide-cracked concrete specimens, on the other hand, exhibited initial splitting tensile strength ranging from 5 to 7.5 MPa, with repaired splitting tensile strength ranging from 2.5 to 3 MPa. The recovery ratio ranged from 40% to 50%. The crack aperture of the concrete significantly influenced the splitting tensile strength recovery ratio, with narrow-cracked concrete demonstrating a higher recovery ratio compared to wide-cracked concrete. This discrepancy may be attributed to the incomplete filling of cracks by calcium carbonate crystals in cases where the crack aperture was larger, resulting in a lower tensile strength recovery ratio.

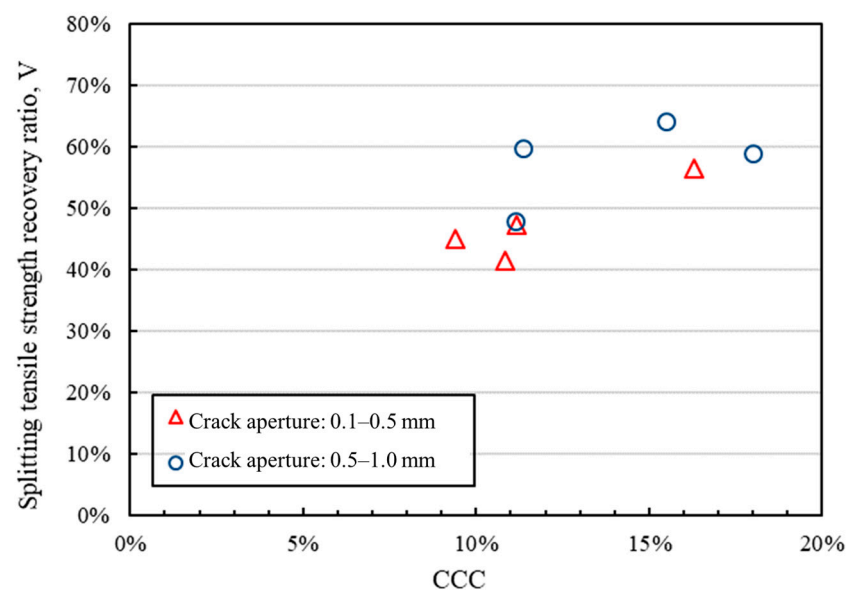


Figure 14. Relationship between splitting tensile strength recovery ratio of concrete and calcium carbonate content in sand columns.

3.2.5. Microstructure

In Figure 15a, the SEM image of narrow-cracked concrete revealed a significant presence of calcium carbonate crystals distributed across the rough crack surface, forming clusters. Upon closer examination in the partially enlarged image on the right, two types of crystals are observable: large polyhedral crystals ranging from 15 to 20 μm in diameter and small spherical crystals measuring between 2 and 3 μm . Notably, the small crystals originate from prefabricated bioslurry, while the large crystals result from the mineralization reaction of the injected cement solution. This varied crystal size distribution enhances the effectiveness of crack and pore filling within the concrete.

In Figure 15b, the SEM image of wide-cracked concrete showed a more uniform distribution of calcium carbonate crystals compared to narrow-cracked concrete. Upon closer inspection in the locally enlarged image on the right, it became evident that the crystals were uniformly polyhedral in shape, with an approximate diameter of 10 μm . These crystals were densely arranged and embedded within each other, contributing to the improved reinforcement of the concrete structure.

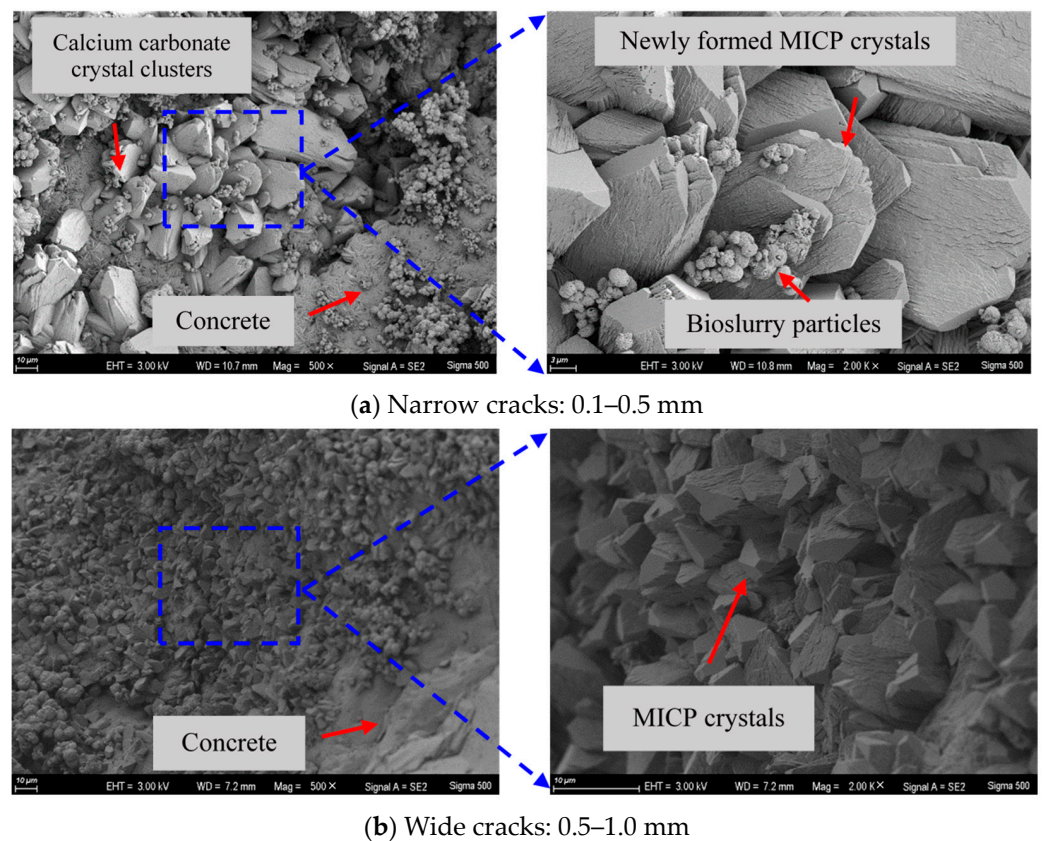


Figure 15. SEM images of MICP in concrete cracks.

4. Conclusions

This study conducted sand particle cementation tests to assess the impact of a novel method (bioslurry + filling particles) on sand particle cementation. Subsequently, it focused on the simultaneous repair of sand particles and concrete cracks to evaluate the feasibility and effectiveness of concurrent repairs and the influence of concrete crack openings on the repair process. The following conclusions were drawn:

(1) Filling particles proved effective in enhancing the unconfined compressive strength and permeability resistance during microbial grouting in unsaturated conditions. Incorporating filling particles significantly improved sand particle cementation, with the permeability of sand columns reinforced with 5% bioslurry + 10% filling particles for 3 days being reduced by an order of magnitude. Moreover, the unconfined compressive strength reached 2.5 MPa, more than twice that of sand columns reinforced with bioslurry alone. The availability of fine calcareous sand particles from various sources at a low cost suggests their potential application in microbial grouting engineering.

(2) SEM images revealed that reinforcement by bioslurry + filling particles effectively enhanced the reinforcement effect. The addition of filling particles provided new nucleation sites for crystallization, forming dense calcium carbonate crystal clusters and cementing sand particles over longer distances, thereby effectively improving the reinforcement effect.

(3) Utilizing bioslurry enabled the simultaneous repair of sand particles and concrete, facilitating sand particle cementation and concrete crack sealing concurrently. A certain shear strength was observed between the sand column and concrete interface. The repair effect was better for narrow-crack concrete than for wide-crack concrete. For narrow cracks with widths between 0.1–0.5 mm, the interfacial shear strength could reach 100 kPa. Additionally, concrete permeability and tensile strength were significantly improved, with the permeability coefficient reduced by more than 80%, and the recovery rate of splitting tensile strength reaching 64.2%. The method of simultaneous grouting repair for sand particles and concrete cracks holds promise for practical applications and provides a

basis for the rapid simultaneous repair of fractured zones in tunnel-surrounding rock and lining cracks.

Author Contributions: Conceptualization, S.Z.; methodology, R.Z.; software, R.Z.; validation, S.Z.; formal analysis, R.Z.; investigation, Z.S.; resources, R.Z.; data curation, S.Z.; writing—original draft preparation, R.Z.; writing—review and editing, C.W. and D.S.; visualization, Z.S.; supervision, C.W.; project administration, C.W.; funding acquisition, C.W. All authors have read and agreed to the published version of the manuscript.

Funding: This research was funded by the National Natural Science Foundation of China (No. 42177141) and the Key Laboratory of Western China's Mineral Resources and Geological Engineering, Ministry of Education, Chang'an University (No. 300102263503).

Institutional Review Board Statement: Not applicable.

Informed Consent Statement: Not applicable.

Data Availability Statement: The data presented in this study are available on request from the corresponding author.

Conflicts of Interest: The authors declare no conflict of interest.

References

- Zhao, Y.; Yang, J.; Zhang, Y. Failure behavior of tunnel lining caused by concrete cracking: A case study. *J. Fail. Anal. Prev.* **2019**, *19*, 1158–1173. [[CrossRef](#)]
- Zhang, N.; Zhu, X.; Ren, Y. Analysis and study on crack characteristics of highway tunnel lining. *Civ. Eng. J.* **2019**, *5*, 1119–1123. [[CrossRef](#)]
- Su, J.; Jie, Y.; Niu, X.; Liu, C.; Liu, X. Mechanical behavior of tunnel lining with cracks at different positions. *Symmetry* **2020**, *12*, 194. [[CrossRef](#)]
- Liu, H.-L.; Xiao, P.; Xiao, Y.; Wang, J.-P.; Chen, Y.-M.; Chu, J. Dynamic behaviors of MICP-treated calcareous sand in cyclic tests. *Chin. J. Geotech. Eng.* **2018**, *40*, 38–45.
- Wu, C.; Chu, J.; Wu, S.; Hong, Y. 3D characterization of microbially induced carbonate precipitation in rock fracture and the resulted permeability reduction. *Eng. Geol.* **2019**, *249*, 23–30. [[CrossRef](#)]
- Qian, C.; Rui, Y.; Wang, C.; Wang, X.; Xue, B.; Yi, H. Bio-mineralization induced by *Bacillus mucilaginosus* in crack mouth and pore solution of cement-based materials. *Mater. Sci. Eng. C* **2021**, *126*, 112120. [[CrossRef](#)] [[PubMed](#)]
- Whiffin, V.S. Microbial CaCO₃ Precipitation for the Production of Biocement. Ph.D. Thesis, Murdoch University, Murdoch, WA, Australia, 2004.
- DeJong, J.T.; Fritzges, M.B.; Nüsslein, K. Microbially induced cementation to control sand response to undrained shear. *J. Geotech. Geoenviron. Eng.* **2006**, *132*, 1381–1392. [[CrossRef](#)]
- Whiffin, V.S.; Van Paassen, L.A.; Harkes, M.P. Microbial carbonate precipitation as a soil improvement technique. *Geomicrobiol. J.* **2007**, *24*, 417–423. [[CrossRef](#)]
- Van Paassen, L.A.; Ghose, R.; van der Linden, T.J.; van der Star, W.R.; van Loosdrecht, M.C. Quantifying biomediated ground improvement by ureolysis: Large-scale biogROUT experiment. *J. Geotech. Geoenviron. Eng.* **2010**, *136*, 1721–1728. [[CrossRef](#)]
- Chu, J.; Stabnikov, V.; Ivanov, V. Microbially induced calcium carbonate precipitation on surface or in the bulk of soil. *Geomicrobiol. J.* **2012**, *29*, 544–549. [[CrossRef](#)]
- Al Qabany, A.; Soga, K. Effect of chemical treatment used in MICP on engineering properties of cemented soils. In *Bio-and Chemo-Mechanical Processes in Geotechnical Engineering: Géotechnique Symposium in Print 2013*; ICE Publishing: London, UK, 2014; pp. 107–115.
- Salifu, E.; MacLachlan, E.; Iyer, K.R.; Knapp, C.W.; Tarantino, A. Application of microbially induced calcite precipitation in erosion mitigation and stabilisation of sandy soil foreshore slopes: A preliminary investigation. *Eng. Geol.* **2016**, *201*, 96–105. [[CrossRef](#)]
- Jiang, N.J.; Soga, K. Erosional behavior of gravel-sand mixtures stabilized by microbially induced calcite precipitation (MICP). *Soils Found.* **2019**, *59*, 699–709. [[CrossRef](#)]
- Wu, C.; Chu, J. BiogROUTing method for stronger bond strength for aggregates. *J. Geotech. Geoenviron. Eng.* **2020**, *146*, 06020021. [[CrossRef](#)]
- Pan, X.; Chu, J.; Yang, Y.; Cheng, L. A new biogROUTing method for fine to coarse sand. *Acta Geotech.* **2020**, *15*, 1–16. [[CrossRef](#)]
- Wu, C.; Song, Z.; Jang, B.A.; Song, H.G.; Ni, P. Strength improvement of rock fractures and aggregates cemented with bio-slurry. *Mater. Lett.* **2021**, *305*, 130866. [[CrossRef](#)]
- Khalik, W.; Ehsan, M.B. Crack healing in concrete using various bio influenced self-healing techniques. *Constr. Build. Mater.* **2016**, *102*, 349–357. [[CrossRef](#)]

19. Choi, S.G.; Wang, K.; Wen, Z.; Chu, J. Mortar crack repair using microbial induced calcite precipitation method. *Cem. Concr. Compos.* **2017**, *83*, 209–221. [[CrossRef](#)]
20. Achal, V.; Mukerjee, A.; Reddy, M.S. Biogenic treatment improves the durability and remediates the cracks of concrete structures. *Constr. Build. Mater.* **2013**, *48*, 1–5. [[CrossRef](#)]
21. Jonkers, H.M. Self healing concrete: A biological approach. In *Self Healing Materials: An Alternative Approach to 20 Centuries of Materials Science*; Springer: Dordrecht, The Netherlands, 2007; pp. 195–204.
22. Jonkers, H.M.; Thijssen, A.; Muyzer, G.; Copuroglu, O.; Schlangen, E. Application of bacteria as self-healing agent for the development of sustainable concrete. *Ecol. Eng.* **2010**, *36*, 230–235. [[CrossRef](#)]
23. *ASTM D2166*; Standard Test Method for Unconfined Compression Strength of Cohesive Soil (Superseded). ASTM International: Conshohocken, PA, USA, 2013.
24. *ASTM C496*; Standard Test Method for Splitting Tensile Strength of Cylindrical Concrete Specimens. ASTM International: Conshohocken, PA, USA, 2017.
25. Al Qabany, A.; Soga, K.; Santamarina, C. Factors affecting efficiency of microbially induced calcite precipitation. *J. Geotech. Geoenviron. Eng.* **2012**, *138*, 992–1001. [[CrossRef](#)]
26. Konstantinou, C.; Biscontin, G.; Jiang, N.J.; Soga, K. Application of microbially induced carbonate precipitation to form bio-cemented artificial sandstone. *J. Rock Mech. Geotech. Eng.* **2021**, *13*, 579–592. [[CrossRef](#)]
27. Cheng, L.; Shahin, M.A. Urease active bioslurry: A novel soil improvement approach based on microbially induced carbonate precipitation. *Can. Geotech. J.* **2016**, *53*, 1376–1385. [[CrossRef](#)]

Disclaimer/Publisher’s Note: The statements, opinions and data contained in all publications are solely those of the individual author(s) and contributor(s) and not of MDPI and/or the editor(s). MDPI and/or the editor(s) disclaim responsibility for any injury to people or property resulting from any ideas, methods, instructions or products referred to in the content.